Nano Energy 48 (2018) 35–43

Contents lists available at ScienceDirect

Nano Energy

journal homepage: www.elsevier.com/locate/nanoen

Full paper

Boosting the performance of lithium batteries with solid-liquid hybrid electrolytes: Interfacial properties and effects of liquid electrolytes

Changhong Wang[a], Qian Sun[a], Yulong Liu[a], Yang Zhao[a], Xia Li[a], Xiaoting Lin[a], Mohammad Norouzi Banis[a], Minsi Li[a], Weihan Li[a], Keegan R. Adair[a], Dawei Wang[a], Jianneng Liang[a], Ruying Li[a], Li Zhang[b], Rong Yang[b], Shigang Lu[b], Xueliang Sun[a,*]

[a] Department of Mechanical and Materials Engineering, University of Western Ontario, 1151 Richmond St, London, Ontario, Canada N6A 3K7
[b] China Automotive Battery Research Institute Co., Ltd., 5th Floor, No. 43, Mining Building, North Sanhuan Middle Road, Haidian District, Beijing 100088, China

ARTICLE INFO

Keywords:
Solid-liquid hybrid electrolyte
Solid-liquid electrolyte interphase
Lithium batteries

ABSTRACT

Solid-state lithium batteries have attracted significant attention recently due to their superior safety and energy density. Nevertheless, the large interfacial resistance has limited the development of SSLBs. To tackle this problem, a general strategy is to add liquid electrolytes (LE) at the interface to form a solid-liquid hybrid electrolyte. However, the effects and interfacial properties of LE in the solid-liquid hybrid electrolyte have not been well-understood. In this work, we quantitatively add LE at the interface to eliminate the large interfacial resistance and study its interfacial properties. As little as 2 μL of LE at the interface enables a hybrid $LiFePO_4$/LATP/Li battery to deliver a specific capacity of 125 mA h g^{-1} at 1 C and 98 mA h g^{-1} at 4 C. Excess LE has no further contribution to the electrochemical performance. Furthermore, the rigid SSE could suppress the formation of lithium dendrites, especially in the case with a high cathode loading (9.1 mg/cm^2), suggesting the feasibility of high energy density SSLBs using Li metal anodes. The interfacial analysis reveals that an interfacial solid-liquid electrolyte interphase (SLEI) was formed at the interface, preventing the reduction of LATP by Li metal, thus ensuring the long-term durability of LATP in LE.

1. Introduction

Solid-state lithium batteries (SSLBs) have attracted great interest recently due to their advantageous energy density and intrinsic safety, which can be realized through the use of lithium metal anodes and solid-state electrolytes (SSEs) [1,2]. To achieve an SSLB, the flammable liquid electrolyte (LE) and separator are replaced by SSEs. Currently, there are three categories of SSEs under development: oxide electrolytes, sulfide electrolytes, and polymer electrolytes [1,3–5]. Compared with sulfide and polymer electrolytes, oxide electrolytes show great potential due to their unique characteristics, such as satisfactory ionic conductivity (nearly 10^{-3} S/cm), good air stability, low toxicity, and low cost [5–7]. However, there are three key challenges impeding the development of oxide electrolyte-based SSLBs. The first challenge is the large interfacial resistance originating from the poor contact between solid-state electrolytes and electrodes. The second challenge is the limited lithium-ion (Li^+) flux inside the electrodes, which arises from the poor contact between particles. The third issue is the chemical instability exhibited by the reduction and oxidation of oxide electrolytes by Li metal and high-voltage cathodes, respectively [8–10].

Over the past decades, several attempts have been made to address the challenges faced by SSLBs, including: (i) co-sintering of active materials with solid-state oxide electrolytes, where some additives, which generally have a low melting point, are employed as a sintering aid to form good contact between electrodes and electrolytes [11,12]; (ii) the development of oxide-polymer (or plastic crystal) hybrid electrolytes, in which improved physical contact between electrodes and electrolytes can be achieved. However, they normally operate at an elevated temperature [13–16]; (iii) solid-liquid hybrid electrolytes, which utilize the wettability of liquid electrolytes to minimize the large contact resistance at the interfaces. Among these options, the use of solid-liquid hybrid electrolytes is one of the most feasible approaches for the development of lithium batteries. For instance, by employing solid-liquid hybrid electrolytes, the plaguing shuttling effect of soluble intermediates in Li-S and Li-Se batteries can be eliminated [17,18]. Furthermore, solid-liquid hybrid electrolytes have been demonstrated to suppress the parasitic side reactions in Li-O_2 batteries [19]. However, the effects and interfacial properties of LE in solid-liquid hybrid electrolyte systems have not been well-understood.

In this work, a quantitative investigation on the volume of LE in

* Corresponding author.
E-mail address: xsun9@uwo.ca (X. Sun).

https://doi.org/10.1016/j.nanoen.2018.03.020
Received 15 February 2018; Received in revised form 6 March 2018; Accepted 7 March 2018
Available online 13 March 2018

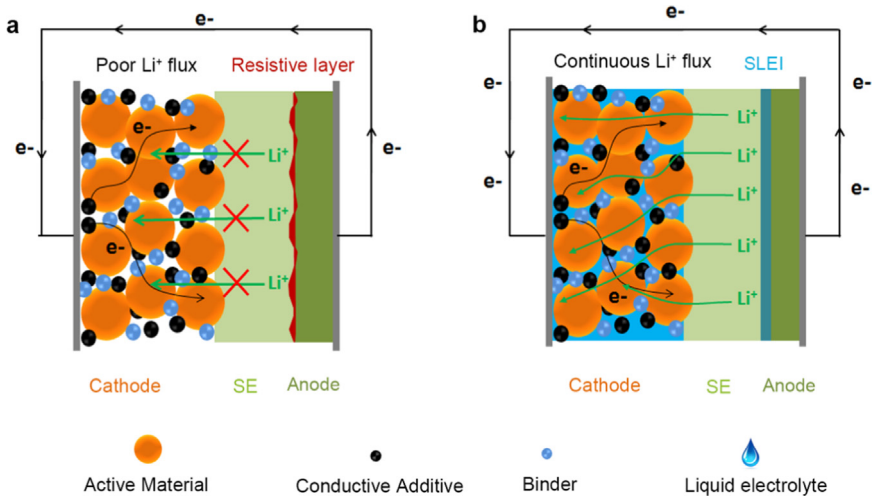

Fig. 1. Schematic diagram of 3D continuous Li^+ ion flux. (a) Illustration of lithium ion and electron fluxes inside the conventional cathode. (b) A trace amount of LE was added to both sides of the SE, filling the pores within the cathode as well as wetting the Li metal surface.

solid-liquid hybrid electrolytes was performed and the interfacial properties of LE in the lithium batteries were conducted. A hybrid lithium battery consists of $LiFePO_4$ as the cathode, a glass ceramic $Li_{1.4}Al_{0.4}Ti_{1.6}(PO_4)_3$ (GC-LATP)/liquid electrolyte ($LiPF_6$ in EC/DMC/DEC) as the hybrid electrolyte, and Li metal as the anode. As a result, the hybrid lithium battery can deliver impressive electrochemical performances, which are even comparable with those of their LE-based counterparts. It was found that the formation of an interfacial solid-liquid electrolyte interphase (SLEI) on the surface of GC-LATP prevents the reduction of GC-LATP by Li metal, and enables the long-term electrochemical durability of GC-LATP in the LE. In addition, the robust SE could suppress the growth of lithium dendrites upon cycling, especially in the case with a high cathode loading (9.1 mg/cm^2), which suggests the feasibility of Li metal in SSLBs with improved safety and high energy density. This investigation can provide great insights into the solid-liquid hybrid electrolytes for lithium-ion batteries with improved safety and energy density.

2. Experimental section

2.1. Synthesis of LATP and glass ceramic LATP (GC-LATP)

Analytical reagent-grade chemicals of Li_2CO_3, Al_2O_3, TiO_2, and $(NH_4)_2HPO_4$ were used as starting materials. Stoichiometric quantities of starting materials were weighed and placed in agate jars. To compensate for the volatility of lithium during the high-temperature annealing process, an excess amount of Li_2CO_3 was added. Ball milling was conducted with ZrO_2 balls and a mass ratio of starting materials: balls of 1:10. Anhydrous ethanol was used as a solvent for wet ball milling. The powders were mixed by planetary ball milling for 2 h at 300 rpm followed by collecting the mixture in a beaker. After drying in a vacuum oven, the powder was transferred to an alumina crucible and heated at 700 °C for 2 h in the air. Then the LATP precursor was obtained by grinding the products with a pestle and mortar. To obtain crystalline LATP, the LATP precursor was compressed into a pellet with a diameter of 1/2 in. Then the pellet was post-annealed at 960 °C for 6 h in the air. The annealed pellets were denoted as LATP for this study. To obtain the glass-ceramic LATP (GC-LATP), the LATP precursor was first mechanically milled at 500 rpm for 80 h. The mass ratio of the LATP powder and balls was 1:20. After the mechanical ball milling, the LATP powder was amorphized and pressed into a pellet. Finally, the pellet was sintered at 960 °C for 6 h in the air. The pellet was named as GC-LATP for this study.

2.2. Materials characterizations

XRD patterns were recorded using a Bruker D8 diffractometer, using Cu Kα radiation. XPS was recorded using Thermo Scientific ESCALAB 250Xi with Al Kα-radiation. The pressure in the analysis chamber was typically 2×10^{-9} Torr during acquisition. Raman spectra were collected using the laser with a wavelength of 532 nm. To measure the ionic conductivity of LATP pellets and GC-LATP pellets, gold electrodes were coated on the pellets by sputtering.

2.3. Electrochemical measurements

$LiFePO_4$ was mixed with acetylene black, and PVDF with a mass ratio of 80:10:10 with N-Methyl pyrrolidone (NMP) as a solvent. The paste was coated with an aluminum foil and dried at 110 °C overnight. Then the $LiFePO_4$ was cut into a disc with a diameter of 10 mm and as the cathode. The regular mass loading of $LiFePO_4$ is 1.5–2 mg/cm^2. The $LiCoO_2$ cathode was also prepared with the same procedure. The electrochemical performances of the $LiFePO_4$ were tested in a coil cell (type CR-2032) assembled in an argon-filled glove box with both moisture and oxygen contents below 1 ppm. Glass ceramic LATP pellets with a thickness of (150–250 μm) were put between the $LiFePO_4$ cathode and the lithium metal anode. Different volumes of the liquid electrolyte (1 M LiPF6 in ethylene carbonate (EC)/dimethyl carbonate (DMC)/diethyl carbonate (DEC) with a volume ratio of 1:1:1), was added at the interfaces between electrodes and the LATP pellet, such as 5 μL, 2 μL, and 1 μL at each interface. A pipette with a metrological range from 0.5 μL to 10 μL was used to quantify the volume of the LE. For comparison, a cell with a $LiFePO_4$ cathode was also assembled with 300 μL liquid electrolyte. The cut-off voltages were set from 2.5 V to 4.1 V. Electrochemical impedance analysis was performed on a biologic electrochemical station with a frequency range from 500 kHz to 100 MHz with an amplitude of 10 mV. All the batteries were tested on the LAND system at room temperature.

3. Results and discussion

Fig. 1 shows a schematic diagram of the strategy used to attenuate the interfacial resistance of SSLBs. The conventional cathode, which consists of active materials, conductive agents, and polymeric binder, is directly coupled with a solid-state electrolyte (SSE) and metallic Li anode, as shown in Fig. 1(a). Due to the poor contact between the SSE and electrode surface, the Li^+ flux becomes inhibited and limits the electrochemical performance. However, using a trace amount of LE to

wet the interface can minimize the interfacial resistance between the electrodes and SSE. Meanwhile, the LE can infiltrate the pores of the cathode, enabling a three-dimensional (3D) continuous Li^+ flux with additional solid-liquid contact, as shown in Fig. 1(b). Furthermore, the addition of LE can induce the formation of an interfacial solid-liquid electrolyte interface (SLEI) on the surface of the solid electrolyte, which can serve as a buffer layer to prevent the reduction of solid electrolytes by Li metal, ensuring the long-term durability of the SSE in LE [8].

To examine the effects of LE in solid-liquid hybrid electrolytes, the oxide electrolyte $Li_{1.4}Al_{0.4}Ti_{1.6}(PO_4)_3$ with a NASICON (acronym for sodium (Na) Super Ionic CONductors) structure was picked due its high ionic conductivity, wide electrochemical window, moderate sintering temperature, and good air stability [20–22]. As reported by Fu et al., LATP shows a bulk conductivity of 1.3×10^{-3} S/cm at room temperature [21]. However, it is widely acknowledged that the large grain boundary resistance of LATP limits its overall ionic conductivity. To resolve this issue, glass ceramic LATP was synthesized by mechanical milling to minimize the grain boundary resistance [23]. The synthesis procedure is described in the experimental section. Briefly, upon thermal annealing at 700 °C, the LATP precursors can be seen to yield large particles in the micrometer size domain, as presented in Fig. 2(a). With mechanical milling, which is known as a vitrification process, the particle size could be reduced, as shown in Fig. 2(b). This sample is denoted as GC-LATP in the following discussion. After pelletizing the precursors followed by post-annealing at 960 °C for 6 h, LATP pellets show a significant amount of pores on the surface, as displayed in Figs. 2(c) and S1. In contrast, the GC-LATP pellets have a densely-packed structure without pores on the surface, as demonstrated in Figs. 2(d) and S1. The densified structure of GC-LATP is due to the amorphization of the precursors during the vitrification process, as evidenced by the XRD patterns in Fig. 2(e). After post-annealing, both LATP and glass ceramic LATP show the high-purity $LiTi_2(PO_4)_3$ phase, as exhibited in Fig. 2(f). It should be noted that a 10% excess of Li_2CO_3 was added to complement the volatile loss of the lithium sources during the post-annealing process. Otherwise, some impurities, such as $AlPO_4$ [23], $Li_4P_2O_7$ [24], will form in LATP, as depicted in the XRD patterns in Fig. S2. It should be highlighted that the LATP precursors still show pure phases even with the scale-up process, as demonstrated in Fig. S3, indicating the feasibility of the mass production of LATP precursors.

To evaluate the ionic conductivity of the as-synthesized LATP, gold electrodes were coated on both sides of the LATP pellets by magnetron sputtering. GC-LATP shows an ionic conductivity of 4.1×10^{-4} S cm^{-1} at room temperature, which is almost one order of magnitude higher than that of LATP (6.1×10^{-5} S cm^{-1}), as exhibited in Fig. S4(a). To obtain their activation energies, the temperature-dependent impedance analysis of LATP pellets was examined by varying the temperature from 20 °C to 100 °C (Fig. S4(c) and (d)). According to the Arrhenius equation, $\sigma(T) = \sigma_0.\exp(-E_a/k_BT)$, where E_a is the activation energy, T is the temperature, k_B is the Boltzmann constant, the activation energies of LATP and GC-LATP are 27.88 kJ/mol and 27.27 kJ/mol, respectively,

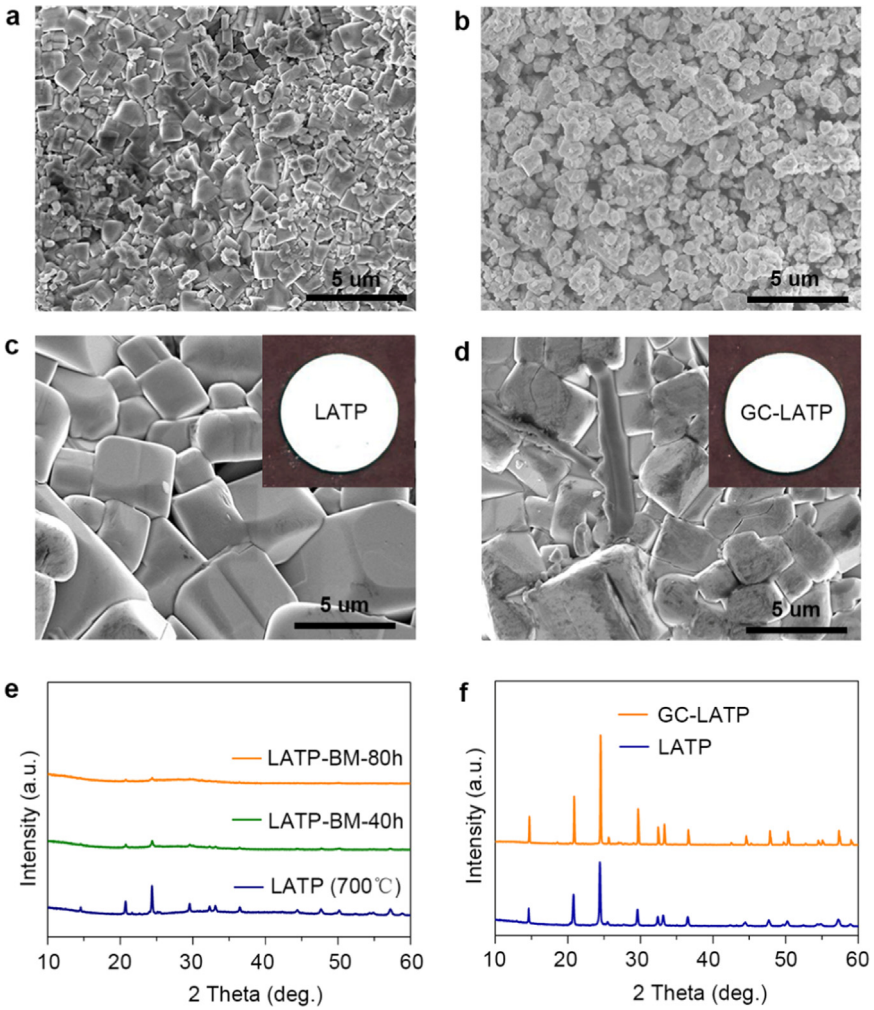

Fig. 2. Comparison between LATP and GC-LATP. (a) The SEM image of the LATP precursor after annealing (700 °C, 2 h). (b) The SEM image of the GC-LATP precursor after mechanical milling for 80 h. (c) The SEM image of the LATP pellet after post-annealing (960 °C, 6 h). (d) The SEM image of the GC-LATP pellet after post-annealing (960 °C, 6 h). (e) XRD spectra of LATP precursors with different ball-milling time. (f) XRD spectra of LATP and GC-LATP pellets after post-annealing (960 °C, 6 h).

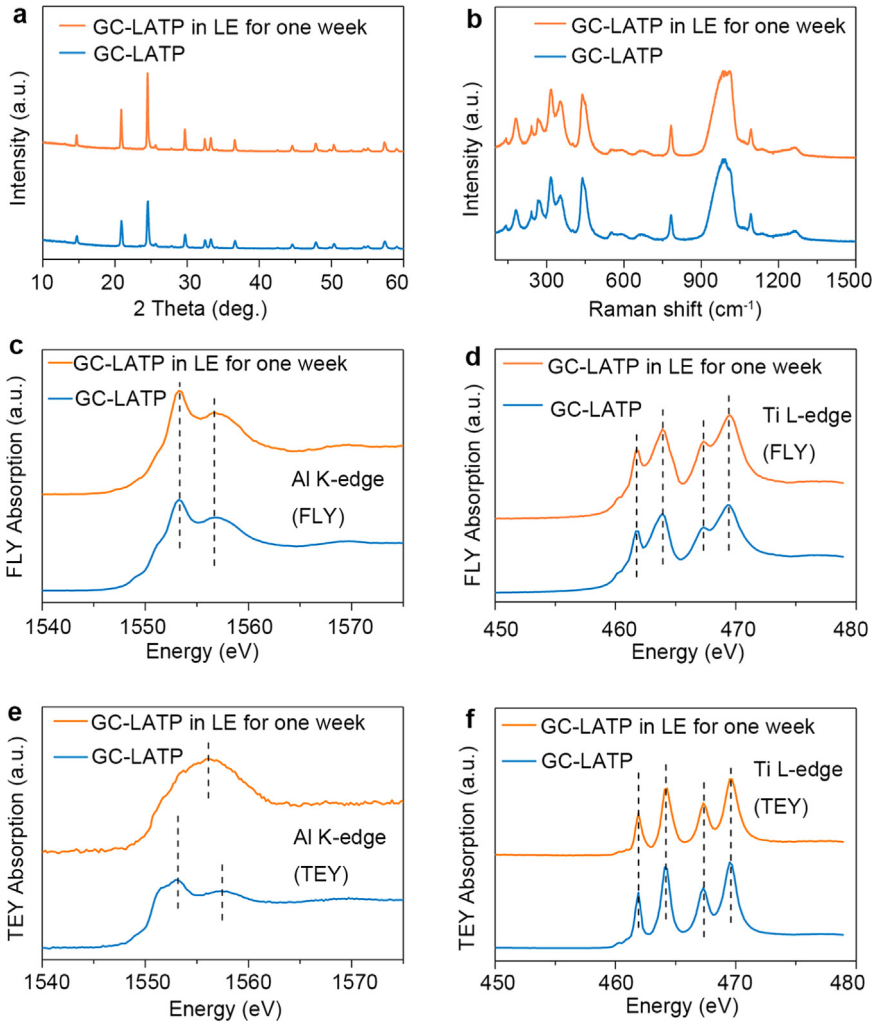

Fig. 3. Chemical compatibility of GC-LATP in carbonate liquid electrolytes. (a) Comparison of XRD patterns of GC-LATP pellets before and after being soaking in LE for one week. (b) Comparison of Raman spectra of GC-LATP pellets before and after being soaking in LE for one week. (c) Al K-edge and (d) Ti L-edge XANES spectra recorded in the FLY mode and (e) Al K-edge & (f) Ti L-edge XANES spectra recorded in the TEY mode of GC-LATP pellets before and after being soaking in LE for one week.

as shown in Fig. S4(b), which are in a good agreement with the results reported in the Refs. [23,25]. For the following study, GC-LATP was selected due to its higher ionic conductivity and lower activation energy as well as increased density, in comparison with those of LATP.

In addition to the high ionic conductivity of the SSEs, the chemical stability of the SE in LE is another important factor for solid-liquid hybrid electrolytes [9,26]. To reveal the chemical stability of GC-LATP in LE, the GC-LATP was soaked in the conventional liquid electrolyte of 1 M $LiPF_6$ in ethylene carbonate (EC)/dimethyl carbonate (DMC)/diethyl carbonate (DEC) with a volume ratio of 1:1:1. After one week, there is no visible change in color of the LE, as shown in Fig. S5. From the XRD patterns of GC-LATP presented in Fig. 3(a), the $LiTi_2(PO_4)_3$ phase was well maintained, indicating that GC-LATP is structurally stable in the LE. Fig. 3(b) exhibits the Raman spectra of the GC-LATP and shows several strong Raman bands appearing in the ranges of 150–500 and 900–1300 cm^{-1}. The bands in the range of 150–500 cm^{-1} should be assigned to symmetrical bending vibrations of PO_4 groups, while those in 900–1100 and 1100–1300 cm^{-1} should be ascribed to the stretching vibrations of PO_3 and PO_2 units, respectively [27]. Again, no new peaks were detected by Raman spectroscopy after soaking of the GC-LATP in the LE for one week, which suggests that the GC-LATP is chemically stable towards common carbonate electrolytes.

To further explore the chemical states of GC-LATP, the normalized Al K-edge and Ti L-edge X-ray absorption near-edge structure (XANES) spectra were examined before and after soaking in LE for one week. Fig. 3(c), (d) and (e), (f) show the XANES spectra recorded in the fluorescence yield (FLY) and total electron yield (TEY) modes, respectively. Based on the different probe depths of the measurement modes (~ 100 nm in the FLY mode and ~ 10 nm in the TEY mode), the chemical states of the bulk and surface regions of GC-LATP can be obtained in FLY and TEY, respectively [28]. No peak shift and shape variation of the Al K-edge was found in the spectra measured in FLY mode, as displayed in Fig. 3(c), further verifying that the bulk of GC-LATP is chemically stable in the LE. In comparison, XANES spectra of the Al K-edge measured in TEY mode showed obvious changes in peak shape (Fig. 3(e)), indicating that AlF_3 is probably formed on the GC-LATP surface [29,30]. This conclusion was further confirmed by the F K-edge XANES spectra in Fig. S6, which also suggests the formation of AlF_3 on the surface. Interestingly, no change was observed in the Ti L-edge spectra measured in both TEY and FLY modes, as shown in Fig. 3(d) and (f). By combining the bulk and interfacial data observed by the XANES spectra, it can be concluded that GC-LATP is stable in carbonate-based liquid electrolytes, which is likely caused by the formation of a passivating AlF_3 layer on the surface. It has been previously reported that the electrochemical performance of hybrid-SSLBs is highly dependent on a good chemical compatibility between the SSE and LE [9,26,31]. Furthermore, the long-term durability of GC-LATP in LE is a prerequisite to enable the commercialization of SSLBs with satisfactory electrochemical performance.

Employing a GC-LATP/LE hybrid electrolyte, $LiFePO_4$-based lithium

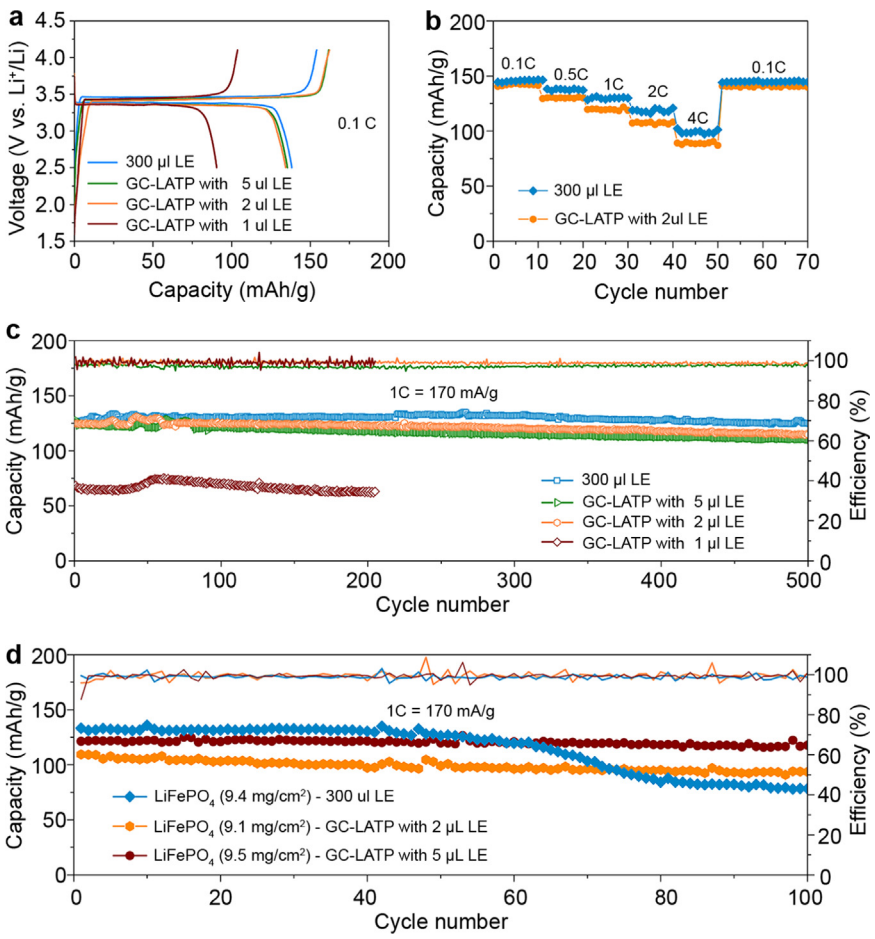

Fig. 4. Electrochemical performances of $LiFePO_4$-based quasi-solid-state lithium ion batteries employing GC-LATP/LE hybrid electrolytes. (a) Charge-discharge curves of $LiFePO_4$ at 0.1 C, (1 C = 170 mA g^{-1}). (b) Rate performance of $LiFePO_4$ at various current densities ranging from 0.1 C to 4 C. (c) Long-term cycling performance of $LiFePO_4$ with quantified volume of LE at a current density of 1 C. (d) The cycling performance of high areal loading $LiFePO_4$ cathodes in conventional LE and GC-LATP/LE hybrid electrolytes.

batteries were fabricated and tested electrochemically. For the first time, how the volume of LE used to wet the SE/electrode surface affects the electrochemical performance of hybrid SSLBs and the formation of the SLEI was investigated. Fig. 4(a) shows the initial charge-discharge curves of the lithium batteries employing GC-LATP/LE hybrid electrolytes with different volumes of LE , which is cycled at 0.1 C (1 C = 170 mA g^{-1}). In the case of 1 µL of LE, the $LiFePO_4$ only delivers a specific capacity of 91 mA h g^{-1}, which suggests that 1 µL of LE is incapable of completely wetting the cathode. From the EIS results shown in Fig. S7, the interfacial resistance of the cell containing 1 µL LE is almost 1000 Ω. By increasing the volume of LE to 2 µL, the interfacial resistance decreases to 275 Ω. The $LiFePO_4$ shows a specific capacity of 134 mA h g^{-1} at 0.1 C and an initial coulombic efficiency of 82.8%, which is only slightly lower than that of their LE-based counterparts (138 mA h g^{-1}, 89.6% coulombic efficiency). This may be caused by the formation of a solid-liquid electrolyte interphase (SLEI) on the surface of GC-LATP [8,32]. In our case, 2 µL of LE is the minimum volume required to enable fully functional lithium batteries with solid-liquid hybrid electrolytes. Fig. 4(b) shows the rate performance of $LiFePO_4$ employing the GC-LATP/LE hybrid electrolyte (2 µL) and conventional LE at different current densities varying from 0.1 C to 4 C. Furthermore, their corresponding charge-discharge curves are presented in Fig. S8(a) and (b). It is surprising that the $LiFePO_4$ delivers a specific capacity of 98 mA h g^{-1} even at the rate of 4 C, which is comparable to the performance of the LE-based counterparts. The decrease in specific capacity at high rates is caused by the larger internal resistance of the lithium batteries with solid-liquid hybrid electroytes. This observation is supported by Fig. S7(a), where the overall resistance of $LiFePO_4$ in the LE is seen to be 169 Ω, which is lower than that of the GC-LATP/LE hybrid electrolyte (275 Ω). Moreover, Fig. 4(c) displays the extended cycling of $LiFePO_4$ with the GC-LATP/LE (2 µL) hybrid electrolyte and yields a specific capacity of 125 mA h g^{-1} at 1 C, which remains as high as 115 mA h g^{-1} after 500 cycles. The hybrid-SSLBs with as little as 2 µL LE show extremely stable cycling performance with a low capacity decay rate of 0.0167% per cycle. Comparatively, the $LiFePO_4$ in conventional LE delivers a specific capacity of 127 mA h g^{-1} at 1 C and maintains a capacity of 125 mA h g^{-1} after 500 cycles with a capacity decay rate of 0.0032%. Compared to 2 µL of LE, 5 µL of LE shows no further contribution to the overall specific capacity but decrease the energy density of hybrid-SSLBs in practice. However, in the case of the hybrid cells with 1 µL LE, the specific capacity is only 68 mA h g^{-1}, which confirms the incomplete wetting of the cathode again.

To obtain high energy density hybrid-SSLBs, cathodes with a high active material loading are required. As demonstrated in Fig. 4(d), the specific capacity of $LiFePO_4$ with high active material loadings (over 9 mg/cm^2) in the conventional LE decreases gradually after 50 cycles. The reason for the capacity fade is believed to be the formation of mossy lithium and/or dendrites due to a large amount of deposited Li metal associated with high loading cathodes [33]. Employing the GC-LATP/LE hybrid electrolytes (2 µL), high-loading $LiFePO_4$ (9.1 mg/cm^2) delivers a stable specific capacity of 100 mA h g^{-1} over 100 cycles at 1 C (1 C = 170 mA/g). Similarly, using GC-LATP/LE hybrid electrolytes (5 µL), high-loading $LiFePO_4$ (9.5 mg/cm^2) delivers a stable specific capacity of 120 mA h g^{-1} over 100 cycles at 1 C. Both cases suggest that the lithium dendrites could be suppressed by the rigid GC-LATP, improving the safety of SSLBs. To show the universal application of the GC-LATP/LE hybrid electrolyte, the hybrid system was also applied to $LiCoO_2$ cathodes, which exhibits an ultra-long cycle stability over 700 cycles as displayed in Fig. S9. To the best of our knowledge, the electrochemical performance of the hybrid-SSLBs in this study is superior to the previously reported literature, [2,6,9,13,31], especially in terms of cyclability and rate performance.

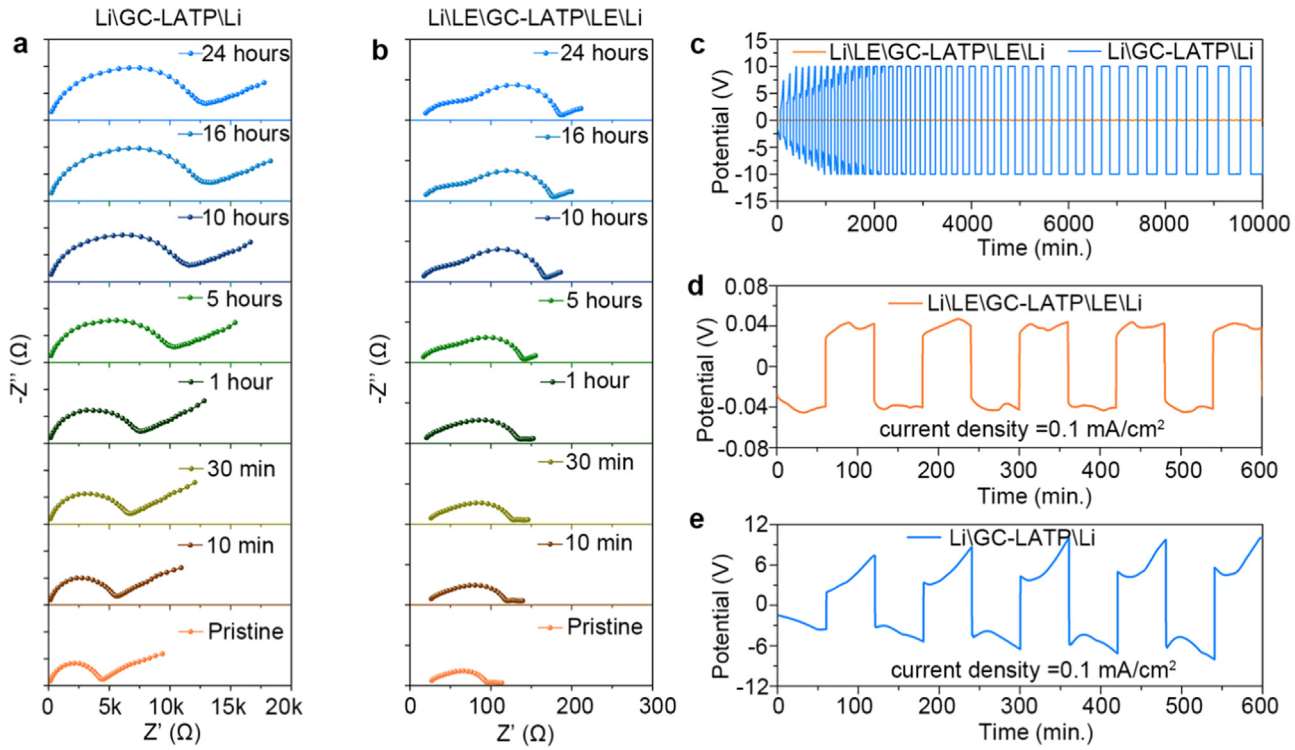

Fig. 5. Evaluation of the GC-LATP and Li metal interface stability. (a) Electrochemical impedance spectra of the symmetric cell with a structure of Li/GC-LATP/Li. (b) Electrochemical impedance spectra of the symmetric cell with a structure of Li/LE/GC-LATP/LE/Li. The volume of LE is 2 μL. (c) Comparison of the plating/stripping profiles between Li/GC-LATP/Li and Li/LE/GC-LATP/LE/Li symmetric cells. (d) The voltage profile of Li/LE/GC-LATP/LE/Li symmetric cells. (e) The voltage profile of Li/GC-LATP/Li symmetric cells.

To reveal the underlying mechanism for the improved performance and cycling stability, a qualitative analysis was further conducted. Firstly, symmetric cells with a structure of Li/GC-LATP/Li were constructed to investigate the interfacial stability between glass ceramic LATP and Li metal. The typical Nyquist plot of Li/GC-LATP/Li is characterized by a high-frequency semicircle and a finite-length Warburg impedance at low frequencies, as exhibited in Fig. 5(a), which indicates the formation of a mixed ion-electron conductor at the interface [34]. The equivalent circuit was shown in Fig. S10(a). The Nyquist plot as a functions of time reveals the interfacial resistance between GC-LATP and Li metal continuously grows from 4470 Ω to 12,983 Ω over a period of 24 h, indicating significant interfacial reactions. The increasing interfacial resistance originates from the reduction of GC-LATP, forming new phases, such as Ti_3P, TiAl, Li_3P, and Li_2O, which are supported by first-principles studies [10,35]. In the case of Li/LE/GC-LATP/LE/Li, the Nyquist plot is dominated by two semicircles, which is typical for a formation of ion-conducting SLEI at the interface between LATP and Li [34]. The corresponding equivalent circuits is shown in Fig. S10(b), in which the first semicircle at high frequency represent the resistance of LATP grain (Rg). The Rint||CPE2 element represents the ion migration in the SLEI layer and dielectric capacitance of the SEI layer.

Comparatively, the large interfacial resistance is dramatically minimized through the use of trace amounts of LE to wet the interface between glass ceramic LATP and Li metal. As displayed in Fig. 5(b), the interfacial resistance decreases to 90 Ω after wetting with 2 μL of LE, which is almost 50 times lower than the original resistance (4470 Ω). Fig. 5(c) presents the plating/stripping profiles of lithium of Li/GC-LATP/Li and Li/LE/GC-LATP/LE/Li symmetric cells, showing that the large overpotential (~ 10 V) of Li/GC-LATP/Li cells could be decreased significantly to 40 mV by adding as little as 2 μL LE on the surface between GC-LATP and Li metal. Fig. 5(d) and (e) shows the galvanostatic cycling of Li/LE/GC-LATP/LE/Li and Li/GC-LATP/Li cells, respectively. After adding 2 μL LE at the interface, the overpotential of Li nucleation is completely eliminated [36]. The separated cycling initial voltage profiles of Li/LE/GC-LATP/LE/Li and Li/GC-LATP/Li cells are presented in Fig. S11. The symmetric cell illustrates that the Li plating/stripping profiles of Li/LE/GC-LATP/LE/Li and Li/GC-LATP/Li cells are completely different, indicating that the underlying mechanism of Li plating/stripping based on SE is different from that in conventional LE [36–38]. Further studies are required to fully understand this phenomenon.

Furthermore, the post-cycling analysis was performed to investigate the solid-liquid electrolyte interphase (SLEI) on the GC-LATP surface. As shown in Fig. S12(b), the clear LATP surface was covered by a thin film layer after 100 cycles, which is believed to be the SLEI layer. SEM coupled with energy dispersive X-ray spectroscopy (EDX) was performed to investigate the composition of the interface. As shown in Fig. S13(a)–(f), elements such as C, P, F, Ti, and Al, are evenly distributed on the surface. The chemical information on the SLEI was further analyzed by X-ray photoelectron spectroscopy (XPS). The full survey XPS spectra of GC-LATP pellets before and after cycling is included in Fig. S14, and the high-resolution spectra of Ti, P, C, and F are displayed in Fig. 6. In comparison with the Ti spectra Fig. 6(a), there is no change after cycling, indicating that the reduction of Ti in GC-LATP by Li metal is prevented by the formation of the SLEI layer [39,40]. Fig. 6(b) shows the high-resolution P spectra before and after cycling, which clearly shows new peaks at around 137 eV, which is resulted from PF_6^-. Fig. 6(c) exhibits the high-resolution spectra of C 1s. After cycling the CO_3^{2-} peak was detected, suggesting Li_2CO_3 forms on the surface of GC-LATP after cycling [8]. As a sharp comparison, the high-resolution F 1s spectra were shown in Fig. 6(d), suggesting that PF_6^- and LiF (or AlF_3) are formed on the surface of GC-LATP after cycling, which did not show up before cycling. To supplement these results, high-resolution O 1s spectra are also presented in Fig. S15. These results strongly suggest that an SLEI layer is formed on the surface of the GC-LATP pellets after electrochemical cycling, and consists of both lithium salts and organic compounds [8].

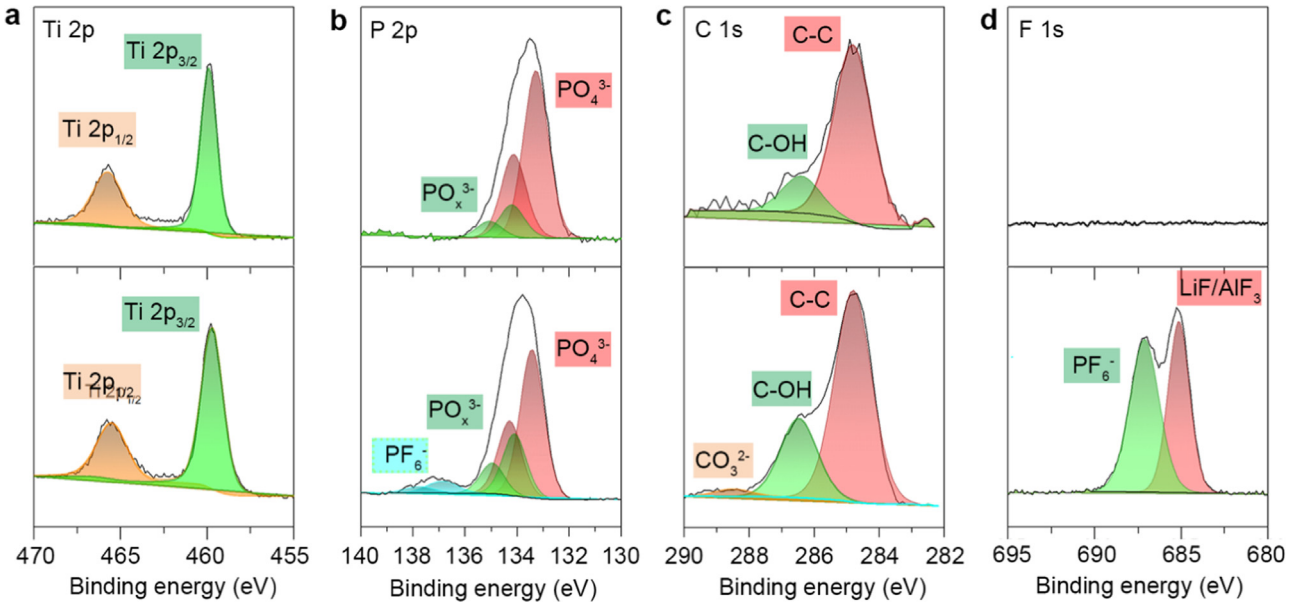

Fig. 6. X-ray photoelectron spectra of GC-LATP pellets before and after electrochemical cycling. (a) Ti 2p. (b) P 2p. (c) C 1s (d) F 1s. Top: before cycling, Bottom: after cycling.

4. Conclusion

A lithium battery with a configuration of $LiFePO_4$/GC-LATP/Li was successfully realized, yielding a specific capacity of 125 mA h g^{-1} when cycled at 1 C and 98 mA h g^{-1} at 4 C. To the best of our knowledge, the electrochemical performances are superior to all previously reported results. The superior electrochemical performance is attributed to the long-term durability of GC-LATP in LE and the formation of the SLEI on the GC-LATP surface, which prevents the reduction of GC-LATP by Li metal and enables a stable cycling performance. Moreover, the robust SE could suppress the growth of lithium dendrites upon cycling, improving the safety and energy density of lithium batteries. Furthermore, we have exemplified the importance of quantitatively controlling the volume of LE to enable high-performance quasi-SSLB systems. This demonstration can help guide future research in solid-liquid hybrid electrolyte systems for SSLBs with improved safety and energy density.

Acknowledgements

This work was supported by Natural Sciences and Engineering Research Council of Canada (NSERC), Canada Research Chair Program (CRC), China Automotive Battery Research Institute, Canada Foundation for Innovation (CFI), the Canada Light Source at University of Saskatchewan (CLS) and University of Western Ontario.

Appendix A. Supplementary material

Supplementary data associated with this article can be found in the online version at http://dx.doi.org/10.1016/j.nanoen.2018.03.020.

References

[1] A. Manthiram, X. Yu, S. Wang, Nat. Rev. Mater. 2 (2017) 16103.
[2] K. Fu, Y. Gong, B. Liu, Y. Zhu, S. Xu, Y. Yao, W. Luo, C. Wang, S.D. Lacey, J. Dai, Y. Chen, Y. Mo, E. Wachsman, L. Hu, Sci. Adv. 3 (2017).
[3] C. Sun, J. Liu, Y. Gong, D.P. Wilkinson, J. Zhang, Nano Energy 33 (2017) 363–386.
[4] J.C. Bachman, S. Muy, A. Grimaud, H.-H. Chang, N. Pour, S.F. Lux, O. Paschos, F. Maglia, S. Lupart, P. Lamp, L. Giordano, Y. Shao-Horn, Chem. Rev. 116 (2016) 140–162.
[5] V. Thangadurai, S. Narayanan, D. Pinzaru, Chem. Soc. Rev. 43 (2014) 4714–4727.
[6] X. Han, Y. Gong, K. Fu, X. He, G.T. Hitz, J. Dai, A. Pearse, B. Liu, H. Wang, G. Rubloff, Y. Mo, V. Thangadurai, E.D. Wachsman, L. Hu, Nat. Mater. 16 (2017) 572–579.
[7] E. Quartarone, P. Mustarelli, Chem. Soc. Rev. 40 (2011) 2525–2540.
[8] M.R. Busche, T. Drossel, T. Leichtweiss, D.A. Weber, M. Falk, M. Schneider, M.-L. Reich, H. Sommer, P. Adelhelm, J. Janek, Nat. Chem. 8 (2016) 426–434.
[9] B. Xu, H. Duan, H. Liu, C.A. Wang, S. Zhong, ACS Appl. Mater. Interfaces 9 (2017) 21077–21082.
[10] Y. Zhu, X. He, Y. Mo, ACS Appl. Mater. Interfaces 7 (2015) 23685–23693.
[11] P. Birke, F. Salam, S. Döring, W. Weppner, Solid State Ion. 118 (1999) 149–157.
[12] S. Ohta, J. Seki, Y. Yagi, Y. Kihira, T. Tani, T. Asaoka, J. Power Sources 265 (2014) 40–44.
[13] W. Zhou, S. Wang, Y. Li, S. Xin, A. Manthiram, J.B. Goodenough, J. Am. Chem. Soc. 138 (2016) 9385–9388.
[14] Z. Zhang, Y. Zhao, S. Chen, D. Xie, X. Yao, P. Cui, X. Xu, J. Mater. Chem. A (2017).
[15] H. Gao, L. Xue, S. Xin, K. Park, J.B. Goodenough, Angew. Chem. Int. Ed. 56 (2017) 5541–5545.
[16] P.-J. Alarco, Y. Abu-Lebdeh, A. Abouimrane, M. Armand, Nat. Mater. 3 (2004) 476–481.
[17] L. Wang, Y. Wang, Y. Xia, Energy Environ. Sci. 8 (2015) 1551–1558.
[18] Y. Zhou, Z. Li, Y.-C. Lu, Nano Energy 39 (2017) 554–561.
[19] L. Li, S.-H. Chai, S. Dai, A. Manthiram, Energy Environ. Sci. 7 (2014) 2630–2636.
[20] R.J. Chen, W.J. Qu, X. Guo, L. Li, F. Wu, Mater. Horiz. 3 (2016) 487–516.
[21] J. Fu, Solid State Ion. 96 (1997) 195–200.
[22] K. Arbi, S. Mandal, J.M. Rojo, J. Sanz, Chem. Mater. 14 (2002) 1091–1097.
[23] X. Xu, Z. Wen, J. Wu, X. Yang, Solid State Ion. 178 (2007) 29–34.
[24] X. Liu, J. Tan, J. Fu, R. Yuan, H. Wen, C. Zhang, ACS Appl. Mater. Interfaces 9 (2017) 11696–11703.
[25] X. Xu, Z. Wen, X. Yang, J. Zhang, Z. Gu, Solid State Ion. 177 (2006) 2611–2615.
[26] S. Wang, Y. Ding, G. Zhou, G. Yu, A. Manthiram, ACS Energy Lett. 1 (2016) 1080–1085.
[27] R. Pikl, D. de Waal, A. Aatiq, A. El Jazouli, Mater. Res. Bull. 33 (1998) 955–961.
[28] W. Huang, A. Marcelli, D. Xia, Adv. Energy Mater. 7 (2017) (1700460-n/a).
[29] S.L.M. Schroeder, N. Weiher, Phys. Chem. Chem. Phys. 8 (2006) 1807–1811.
[30] I. Grohmann, A. Hess, E. Kemnitz, W. Fentrup, W.E.S. Unger, J. Wong, M. Rowen, T. Tanaka, M. Froba, J. Mater. Chem. 8 (1998) 1453–1457.
[31] T. Liu, Y. Ren, Y. Shen, S.-X. Zhao, Y. Lin, C.-W. Nan, J. Power Sources 324 (2016) 349–357.
[32] Y. Kato, S. Hori, T. Saito, K. Suzuki, M. Hirayama, A. Mitsui, M. Yonemura, H. Iba, R. Kanno, Nat. Energy 1 (2016) 16030.
[33] X.-B. Cheng, R. Zhang, C.-Z. Zhao, Q. Zhang, Chem. Rev. 117 (2017) 10403–10473.
[34] P. Bron, B. Roling, S. Dehnen, J. Power Sources 352 (2017) 127–134.
[35] Y. Zhu, X. He, Y. Mo, J. Mater. Chem. A 4 (2016) 3253–3266.
[36] K. Yan, Z. Lu, H.-W. Lee, F. Xiong, P.-C. Hsu, Y. Li, J. Zhao, S. Chu, Y. Cui, Nat. Energy 1 (2016) 16010.
[37] K.-H. Chen, K.N. Wood, E. Kazyak, W.S. LePage, A.L. Davis, A.J. Sanchez, N.P. Dasgupta, J. Mater. Chem. A 5 (2017) 11671–11681.
[38] K.N. Wood, E. Kazyak, A.F. Chadwick, K.-H. Chen, J.-G. Zhang, K. Thornton, N.P. Dasgupta, ACS Cent. Sci. 2 (2016) 790–801.
[39] C. Ye, L. Zhang, C. Guo, D. Li, A. Vasileff, H. Wang, S.-Z. Qiao, Adv. Funct. Mater. 27 (2017) 1702524.
[40] F. Xie, L. Zhang, D. Su, M. Jaroniec, S.-Z. Qiao, Adv. Mater. 29 (2017) 1700989.

Changhong Wang is currently a Ph.D. candidate in Prof. Xueliang (Andy) Sun's Group at the University of Western Ontario, Canada. He got his B.S. in applied chemistry from University of Science and Technology of Anhui in 2011 and obtained his M.S. degree in materials engineering from University of Science and Technology of China in 2014. After graduation, he also served as a research assistant in Singapore University of Technology and Design from 2014 to 2016. Currently, his research interests include solid-state sulfide electrolytes, all-solid-state LIBs and Li-S batteries, and memristors.

Dr. Qian Sun is a postdoctoral associate in Prof. Xueliang (Andy) Sun's Group at the University of Western Ontario (Western University), Canada. He received his B.S. degree in Chemistry in 2006, M.S. degree in Physical Chemistry in 2009, and Ph.D. degree in Applied Chemistry in 2013 under the supervision of Prof. Dr. Zheng-Wen Fu on the study of Li-/Na-ion batteries and Na-air batteries, all at Fudan University, China. He joined Prof. Sun's group in 2013 and his current research interests focus on Na-air, Na-ion, and room temperature Na-S batteries as well as solid-state Li/Na batteries.

Dr. Yulong Liu is currently postdoctoral fellow in Prof. Xueliang (Andy) Sun' Nanomaterials and Energy Group at the University of Western Ontario, Canada. He received his Bachelor degree from Central South University, China, in 2010, and Master degree in 2013. In 2017, he obtained his Ph.D. degree in Materials Science and Engineering from University of Western Ontario. His research interests include nanomaterials for lithium ion batteries, especially $LiFePO_4$ (in collaboration with *Johnson Matthey Inc.*, previous Phostech), and the development of the solid state batteries.

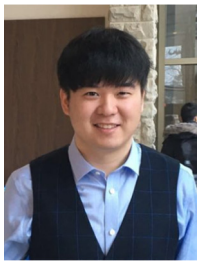

Yang Zhao is currently a Ph.D. candidate in Prof. Xueliang (Andy) Sun's Group at the University of Western Ontario, Canada. He received his B.S. degree and M.S. degree in Chemical Engineering and Technology from Northwestern Polytechnical University (Xi'an, China) in 2011 and 2014, respectively. His current research interests focus on atomic/molecular layer deposition in the application of lithium/sodium ion batteries and all solid state batteries.

Dr. Xia Li is a postdoctoral fellow in Prof. Xueliang (Andy) Sun's Nanomaterials and Energy Group. She received her Ph.D. degree at the University of Western Ontario, Canada. Her current research interests focus on development of advanced nanomaterials for lithium-sulfur batteries, sulfur based solid-state electrolyte.

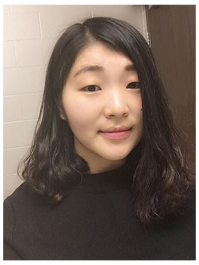

Xiaoting Lin is currently a Ph.D. candidate in Prof. Xueliang (Andy) Sun's group at the University of Western Ontario, Canada. She received her B.S. degree in Applied chemistry in 2012 from Liaocheng University and obtained her M.S. degree in Physical Chemistry in 2016 from Ningbo University. Currently, her research interests focus on development of advanced nanomaterials for Na-O_2 batteries as well as solid-state Na-O_2 batteries.

Dr. Mohammad Norouzi Banis is research engineer in Prof. Xueliang (Andy) Sun's group at University of Western Ontario, Canada. He received his Ph.D. degree in 2013 in Materials Science and Engineering from Western University, on the study of nanostructured low temperature fuel cells and application of x-ray absorption spectroscopy in energy related systems. His current research interests include study of metal ion, metal air and nanocatalysts via in-situ synchrotron based techniques.

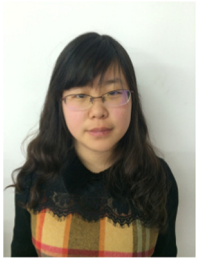

Minsi Li received the B.S. degree from the University of Science and Technology of China, Hefei, Anhui, P.R. China in 2016. She is currently a Ph.D. candidate at Prof. Xueliang (Andy) Sun's Nanomaterials and Energy Group at the University of Western Ontario, Canada. Her research interests mainly include preparation and characterization of nanomaterials for sodium-ion batteries.

Dr. Weihan Li completed his doctorate in material sciences under the supervision of Prof. Yan Yu at the University of Science and Technology of China, Hefei in 2016. He is currently a postdoctoral fellow at Prof. Xueliang (Andy) Sun's Nanomaterials and Energy Group at the University of Western Ontario, Canada. His research interests mainly include synthesis and application of nanomaterials for lithium-ion battery and sodium-ion battery.

Keegan R. Adair received his B.Sc. in chemistry from the University of British Columbia in 2016. He is currently a Ph.D. candidate in Prof. Xueliang (Andy) Sun's Nanomaterials and Energy Group at the University of Western Ontario, Canada. Keegan has previously worked on battery technology at companies such as E-One Moli Energy and General Motors. His research interests include the design of nanomaterials for lithium metal batteries and nanoscale interfacial coatings for battery applications.

Dr. Dawei Wang obtained his Bachelor at Dalian University of Technology in 2009, and received his Ph.D. from Xiamen University in 2015. Later he worked as a visiting scholar at Brookhaven Nation Laboratory. He currently is a postdoctoral associate at University of Western Ontario. His research interests include solid-state electrolytes, solid-state LIBs and high-energy cathode materials.

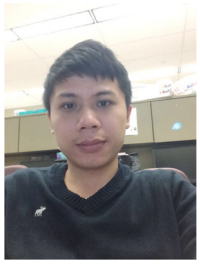

Jianneng Liang is currently a Ph.D. candidate in the department of Mechanical and Materials Engineering at the University of Western Ontario, Canada. He got his B.S. in metallurgical engineering in 2015 from Central South University, China. Currently, his research interests include solid-state polymer electrolytes, hybrid electrolyte, all-solid-state LIBs and Li-S batteries, and the interfacial study in all-solid-state batteries.

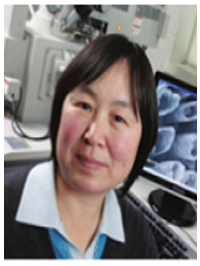

Ruying Li is a research engineer at Prof. Xueliang (Andy) Sun's Nanomaterial and Energy Group at the University of Western Ontario, Canada. She received her master in Material Chemistry under the direction of Prof. George Thompson in 1999 at University of Manchester, UK, followed by work as a research assistant under the direction of Prof. Keith Mitchell at the University of British Columbia and under the direction of Prof. Jean-Pol Dodelet at l'Institut national de la recherché scientifique (INRS), Canada. Her current research interests are associated with synthesis and characterization of nanomaterials for electrochemical energy storage and conversion.

Dr. Li Zhang is currently a senior scientist of China Automotive Battery Research Institute Co., Ltd., Beijing, China. He received his Ph.D. degree in Electrochemistry from University of Science & Technology Beijing, China in 2009. He has more than 10 years of power sources experience with expertise in battery materials as well as electrode design. Currently, his research interests include solid-state electrolytes, all-solid-state Li-AIR and Lithium batteries.

Dr. Rong Yang received his Ph.D. degree in inorganic chemistry from Peking University in 2011. He is currently a senior engineer in China Automotive Battery Research Institute. His research interests are focused on cathode materials for lithium-ion batteries, solid-state lithium ion conductors and solid-state lithium-ion batteries.

Dr. Shigang Lu is Vice president of China Automotive Battery Research Institute Co., Ltd. He has the responsibility for technology innovations in the area of automotive battery application. He has extensive experience in many energy research areas including fuel cells, and lithium-ion batteries. Dr. Lu received her Ph.D. degree in Chemistry from Moscow State University in 1993. He has extensive experience in novel material processing techniques for automotive battery applications. His current research interests include new energy electrochemistry, lithium ion battery and related materials, solid state battery and related materials.

Prof. Xueliang Sun is a Canada Research Chair in Development of Nanomaterials for Clean Energy, Fellow of the Royal Society of Canada and Canadian Academy of Engineering and Full Professor at the University of Western Ontario, Canada. Dr. Sun received his Ph.D. in materials chemistry in 1999 from the University of Manchester, UK, which he followed up by working as a postdoctoral fellow at the University of British Columbia, Canada and as a Research Associate at L'Institut National de la Recherche Scientifique (INRS), Canada. His current research interests are focused on advanced materials for electrochemical energy storage and conversion, including electrocatalysis in fuel cells and electrodes in lithium-ion batteries and metal-air batteries.